

## Article

# Effect of Air Parameters on LiCl-H<sub>2</sub>O Film Flow Behavior in Liquid Desiccant Systems

Yue Lyu <sup>1,2,\*</sup>, Yonggao Yin <sup>3</sup> and Jingjing Wang <sup>1,2</sup>

<sup>1</sup> School of Environmental & Municipal Engineering, Lanzhou Jiaotong University, Lanzhou 730070, China; wangjingjing@mail.lzjtu.cn

<sup>2</sup> Key Laboratory of Yellow River Water Environment in Gansu Province, Lanzhou Jiaotong University, Lanzhou 730070, China

<sup>3</sup> School of Energy and Environment, Southeast University, Nanjing 210096, China; y.yin@seu.edu.cn

\* Correspondence: lvyuelzjt@163.com; Tel.: +86-19993090805

**Abstract:** The wettability and stability of a solution's film on the filler surface are the key factors determining heat and mass transfer efficiency in liquid desiccant air conditioning systems. Therefore, this study investigates the effects of different air parameters on the flow behavior of a lithium chloride solution's film. The effects of air velocity, air flow pattern, and pressure on the wettability and critical amount of spray are discussed. The results show that the main mechanism by which the air velocity affects the wettability is that the shear stress generated by the direction of the air velocity disperses the direction of the surface tension and weakens its effect on the liquid film distribution. In addition, in the counter flow pattern, the air flow blocks the liquid film from spreading longitudinally and destroys the stability of the liquid film at the liquid outlet, which increases the critical amount of spray. The pressure distribution is similar under different operating pressures when the flow is stable; thus, pressure has little effect on wettability. The simulation results under 8 atm are compared with the experimental results. It is found that the sudden increase in the amount of moisture removal when the amount of spray changes from 0.05 to 0.1 m<sup>3</sup>/(m·h) in the experiment is caused by the change in the liquid film flow state. In addition, the results show that within the range of air flow parameters for the liquid desiccant air conditioning system, air flow shear force is not the main factor affecting the stability of the solution's film, and there is no secondary breakage of the solution's film during the falling-film flow process.

**Keywords:** liquid desiccant; compressed air; lithium chloride solution; wettability; stability



**Citation:** Lyu, Y.; Yin, Y.; Wang, J. Effect of Air Parameters on LiCl-H<sub>2</sub>O Film Flow Behavior in Liquid Desiccant Systems. *Buildings* **2024**, *14*, 1474. <https://doi.org/10.3390/buildings14051474>

Academic Editors: Yuehong Su and Christopher Yu-Hang Chao

Received: 16 March 2024

Revised: 12 May 2024

Accepted: 16 May 2024

Published: 18 May 2024



**Copyright:** © 2024 by the authors. Licensee MDPI, Basel, Switzerland. This article is an open access article distributed under the terms and conditions of the Creative Commons Attribution (CC BY) license (<https://creativecommons.org/licenses/by/4.0/>).

## 1. Introduction

Compressed air is widely used in various industries as both a power source as well as a process gas source for various applications such as drying and pneumatics [1,2]. However, compressed air can be harmful to production processes when its humidity is too high, leading to problems such as reducing electrical insulation and causing valve corrosion [3]. As the use of liquid desiccants is advantageous in lowering energy costs [4–6], a new method of compressed air drying using liquid desiccant has been proposed. Studies have shown that this system could effectively use the waste heat of air compressors [7,8]. However, because the liquid desiccant systems are still in the development stage, there are still some shortcomings that make them difficult to be applied. First of all, poor heat and mass transfer will make the device huge [9]. Secondly, studies have shown that droplet entraining will occur when there is gas–liquid contact, resulting in the corrosion of indoor surfaces [10]. Therefore, controlling droplet entrainment effectively while improving heat and mass exchange efficiency is the key to optimizing liquid desiccant systems. The current research on optimizing the performance of this new method has only focused on system optimization and control strategies [11,12]. The solution flow behavior on the surface of the filler is an important part in the dehumidification and regeneration processes. The wettability of the

solution's film determines the heat and mass transfer efficiency [13–15], and the stability of the solution's film determines the droplet entrainment. Therefore, it is necessary to systematically study the solution flow behavior during dehumidification/regeneration processes.

In terms of liquid film wettability, due to the numerous variables of a solution's falling-film process in the liquid desiccant air conditioning system, much work is required for its theoretical analysis and experimental research. With the development of computer technology, computational fluid dynamics (CFD) has become an effective method for studying such problems. Sakhnov et al. [16] researched the effect of the contact angle on the spreading of a refrigerant mixture over a vertical cylinder using CFD. They established mathematical models of R21 and R114 refrigerant mixtures flowing over a vertical cylinder, which were in good agreement with the experimental results [17]. Tan et al. [18] studied the effect of liquid viscosity and surface tension on surface wettability. They simulated the flow behavior of several fluids (e.g., ethylene glycol, and acetone) using a volume of fluid (VOF) model and proposed a formula for predicting the effective interface area ratio. These studies indicate that the VOF model is suitable for capturing the gas–liquid two-phase flow interface in simulations. However, in these studies, the gas-phase parameters are ignored due to the small flow rate. Wen et al. [19] proposed a three-dimensional model to describe the shrinkage of the liquid film during falling-film flow on a plate and verified the accuracy of the model through experiments. The results showed that the poor wettability and mass transfer resistance of the air affected the mass transfer capacity, but they did not elaborate on the effect of the air parameters on wettability. At present, it is necessary to maintain a large amount of solution spray to ensure sufficient wetting. However, a larger amount of spray will consume more pump power and may cause droplet carrying problems. Zhang et al. [20] argued that there must be a reasonable value for the solution flow rate, but their research also did not determine the reasonable amount of spray to ensure adequate wetting. From the above studies, it can be seen that the CFD method can be used to conveniently and accurately study a solution's film wettability on the surface of a filler, but the study of the influence of air parameters on a solution's film wettability is still scarce.

In terms of the stability of the liquid film, previous studies have shown that the liquid film may break due to the shear force of the airflow [21]. Wang [22] believes that a wavy liquid film drawn into the airflow is mainly controlled by shear force and surface tension. When the shear force causes the extreme deformation of the interface, it will cause a certain section of the wave to break. In addition, studies have shown that droplets can splash and form microdroplets when they collide with the liquid film. Dai et al. [23] used the coupled level set and VOF method to simulate the morphological evolution and splashing process of liquid droplets impacting an inclined liquid film. They summarized the main water splashing mechanism caused by droplet impact on a liquid film (with water in the liquid phase) as follows: the water splashes in the first half of the liquid are mainly caused by the neck jet resulting from pressure difference, whereas the water splashes in the second half are formed by the change in the direction of the flow of the impacted liquid film. From the above studies, the fragmentation of liquid films is related to the shear force of the air flow, and the impact velocity of droplets in the secondary fragmentation of liquid films is also affected by the incoming air flow velocity. However, most of these studies on the stability of liquid films focused on water, and the research on salt solutions is still scarce.

Based on the discussion above, previous studies of surface wettability have focused on solution properties and filler properties. However, gas-phase parameters also affect the wettability in the gas–liquid falling-film flow for liquid desiccant processes. Especially for compressed air drying systems using liquid desiccants, whether high pressure air will have an effect on the wettability needs to be further discussed. In addition, studies show that air parameters are one of the key factors affecting the stability of the liquid film. However, in these studies, the working fluid used is mostly water, the physical properties of which differ greatly from those of the solution. And the air conditions are also not the same. Therefore, studying the influence of air parameters on the stability of a solution's film according to the working condition and working fluid of liquid desiccant air conditioning

systems is the key to further control droplet entrainment and optimize the systems. At present, halogen salt solutions such as lithium chloride, lithium bromide, and calcium chloride solutions are often used as liquid desiccants in liquid desiccant air conditioning systems. Among them, a lithium chloride solution ( $\text{LiCl-H}_2\text{O}$ ) has the lowest surface partial pressure of water vapor and a low crystallization risk, so it has the highest system efficiency as a liquid desiccant. Therefore, this study takes  $\text{LiCl-H}_2\text{O}$  as the working fluid to explore the air parameters affecting the solution distribution in a liquid desiccant. The effect of the air velocity, the gas–liquid flow pattern, and the gas pressure on the wettability of the solution’s falling film is summarized, and the corresponding critical amount of spray is discussed, which provides a theoretical reference for choosing the amount of spray and the optimal air parameters. The causes of liquid film breakage during the flow process are analyzed, which provides a theoretical basis for further controlling droplet entrainment.

## 2. Materials and Methods

### 2.1. Physical Model

Figure 1 shows the physical model of the air–solution flow channel. The corresponding dimensions and structural vertices are marked in the figure. The dimensions of the falling-film plates remained the same as those in the previous study [24]. The size of the channel is  $50 \times 60 \times 7 \text{ mm}^3$ , and the filler surface is at an angle of  $60^\circ$  relative to the horizontal. The size of the solution inlet is  $0.4 \times 50 \text{ mm}^2$ , which is calculated using the Nusselt film thickness theory. The position of the air inlet and outlet are opposite in the cases of parallel flow and counter flow, with the corresponding boundary conditions for the two flow patterns are shown in Tables 1 and 2, respectively. For parallel flow, the size of the air inlet is  $6.6 \times 50 \text{ mm}$ , which is the channel size minus the solution inlet size. For counter flow, as the liquid film thickness at the bottom becomes thicker with the development of the flow, to ensure that the air inlet does not coincide with the liquid film (causing flooding in the counter flow case), the size of the air inlet is set to half the channel size, which is  $3.5 \times 50 \text{ mm}$ . Therefore, the size of the solution outlet for the counter flow case is  $3.5 \times 50 \text{ mm}$ , which is the channel size minus the air inlet size. As the size of the solution inlet for the counter flow case is the same as that for the parallel flow case, the size of the air outlet is  $6.6 \times 50 \text{ mm}$ .

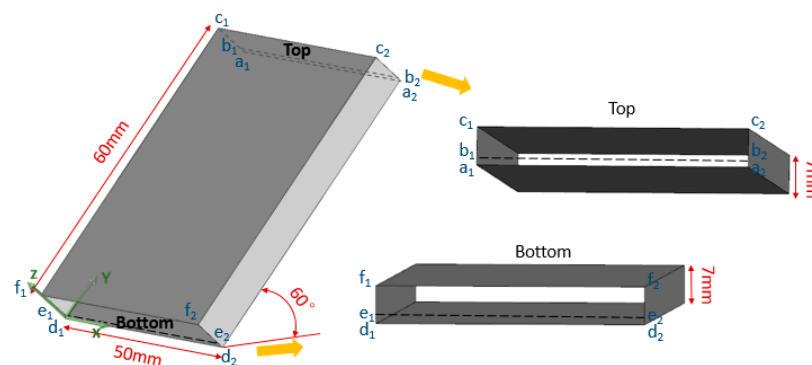


**Figure 1.** A physical model of the air–solution flow channel.

**Table 1.** The boundary condition settings for the parallel flow pattern.

Face	Boundary Condition
$a_1b_1b_2a_2, b_1c_1c_2b_2$	Velocity inlet
$f_1e_1e_2f_2, e_1d_1d_2e_2$	Pressure outlet
$c_1f_1f_2c_2, c_2f_2d_2a_2, a_1d_1f_1c_1, a_1d_1d_2a_2$	No-slip wall

**Table 2.** The boundary condition settings for the counter flow pattern.

Face	Boundary Condition
$a_1b_1b_2a_2, f_1e_1e_2f_2$	Velocity inlet
$b_1c_1c_2b_2, e_1d_1d_2e_2$	Pressure outlet
$c_1f_1f_2c_2, c_2f_2d_2a_2, a_1d_1f_1c_1, a_1d_1d_2a_2$	No-slip wall

## 2.2. Mathematical Modeling

In this paper, Fluent (holding by Ansys in the Canonsburg, PA, United States) is used for the simulation, in which it is important to simulate the change in the interface of the air–solution flow. Compared with other interface capturing methods [25,26], the convergence and mass conservation of the VOF method is superior [27,28]; therefore, it is used in this study to simulate the falling-film flow. The VOF method defines a volume fraction in a cell as  $\alpha$ , which follows Equation (1):

$$\alpha_s + \alpha_a = 1, \quad (1)$$

where  $\alpha_s$  is the volume fraction of the solution, and  $\alpha_a$  is the volume fraction of the air.

The momentum is defined as follows:

$$\frac{\partial(\rho v)}{\partial t} + \nabla(\rho v v) = -\nabla p + \nabla \cdot [\mu(\nabla v + \nabla v^T)] + \rho g + F_{vol}, \quad (2)$$

where  $\rho$  is the density,  $\mu$  is the viscosity, and  $F_{vol}$  is the volume force, which reflects the effect of surface tension.

The continuum surface force model [29] is used to simulate the surface tension. In this model,  $F_{vol}$  is defined as follows:

$$F_{vol} = \sum_{i < j} \sigma_{ij} \frac{\alpha_i \rho_j \kappa_j \nabla \alpha_j + \alpha_j \rho_i \kappa_i \nabla \alpha_i}{\frac{1}{2}(\rho_i + \rho_j)}, \quad (3)$$

where  $\sigma$  is the surface tension coefficient, and  $\kappa$  is the curvature.

Because the air flow is turbulent in this study, the viscous model is chosen as the standard k-epsilon model. To solve the coupling of pressure and velocity, the SIMPLE method is used.

The surface wettability of the filler surface is expressed by the wetting ratio (WR), which is defined as follows:

$$WR = \frac{A_w}{A_b}, \quad (4)$$

where  $A_w$  is the projection area of the solution's film on the filler surface, and  $A_b$  is the area of the filler surface.

A flat falling film is usually realized by overflow, corresponding to the liquid phase inlet of the model in this study, which has a line shape. Therefore, when analyzing the solution flow behavior, the amount of spray of the solution is expressed by the volumetric flow rate per unit of length per unit of time. The amount of spray (SP) is defined as follows:

$$SP = \frac{Q_s}{W} \times 3600 \quad (5)$$

where  $Q_s$  is the volumetric flow rate of the solution, and  $W$  is the inlet width.

The ranges of the gas-phase parameters are selected according to the liquid desiccant evaporative cooling air conditioning system, the liquid desiccant system driven by a heat pump [24], and the compressed air drying system using a liquid desiccant [7]. The conditions of the LiCl solution in this study are the most unfavorable conditions, as shown in Table 3. To ensure the accuracy and speed of the simulation results, the grid is divided into three different densities and we do the same simulation, with grid numbers of 168,000,



228,000, and 288,000. After a grid independence verification, the mesh with 228,000 grids is selected. The accuracy of the mathematical model in this simulation has been verified in previous studies.

**Table 3.** The LiCl solution's conditions.

Process	Concentration (%)	Temperature (°C)
Dehumidification	35	20
Regeneration	30	60

### 2.3. Experimental Methods

A schematic and physical diagrams of the flat plate falling-film experimental device are shown in Figures 2 and 3, respectively. The names of each component are marked in the figures. The device comprises an arched organic glass plate forming two symmetrical falling-film surfaces. The falling-film surfaces and the shell form two gas–liquid two-phase flow channels. The channels are rectangular channels with a width of 15 mm. The flat parts of the arched glass plate in the channels are treated with surface modification and used as filler surfaces. Therefore, the filler surfaces inside the channels are flat surfaces, corresponding to the physical model in the simulation.

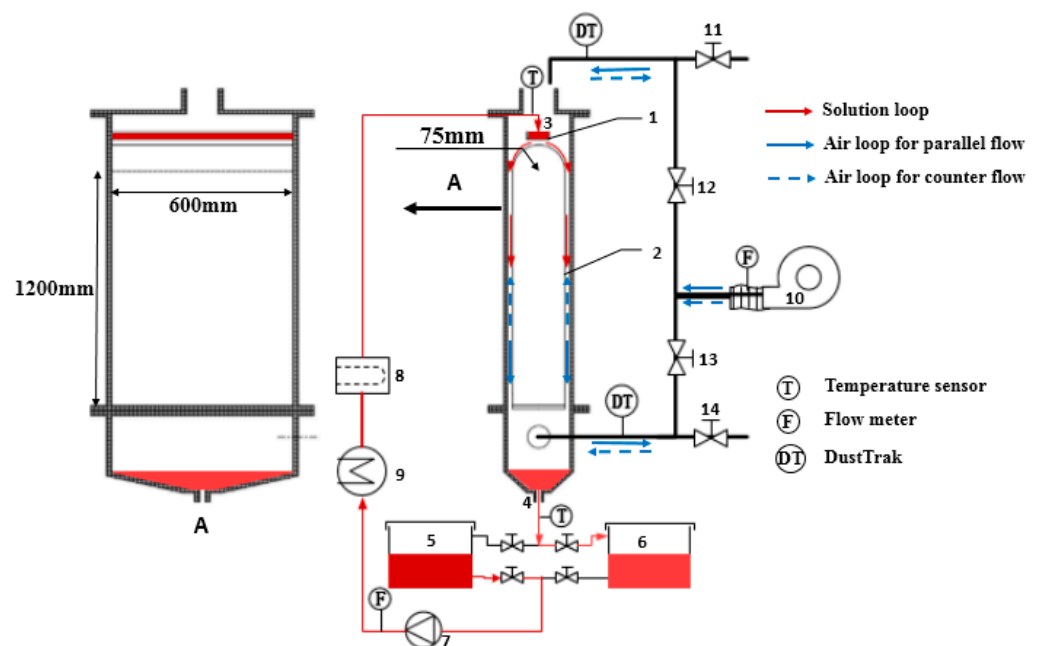


**Figure 2.** A schematic of the flat falling-film experimental device: 1, the liquid distributor; 2, the falling-film plate; 3, the solution inlet; 4, the solution outlet; 5, tank A; 6, tank B; 7, the solution pump; 8, the cooler; 9, the electric heater; 10, the fan; 11, valve A; 12, valve B; 13, valve C; 14, valve D.

According to the liquid desiccant evaporative cooling air conditioning system, the liquid desiccant system driven by a heat pump and a compressed air drying system using liquid desiccant, the experimental conditions are shown in Table 4.

In order to ensure a high measurement accuracy and a lower cost, the measuring range of the measuring equipment is usually about 1.5–2 times the required measuring range. Considering the range of the solution temperature, the solution flow rate and air flow rate to be measured in the experiment (as shown in Table 4), and the relevant parameters of the actual products, the measuring equipment adopted in this study are shown in Table 5. The table also presents the specific parameters of the measurement equipment. The labels T and F in Figure 2 represent K-type thermocouples, and micro flow turbine sensors and gas

vortex flow meters are used to measure the temperature and the flow rate of the solution and air flow rate, respectively.

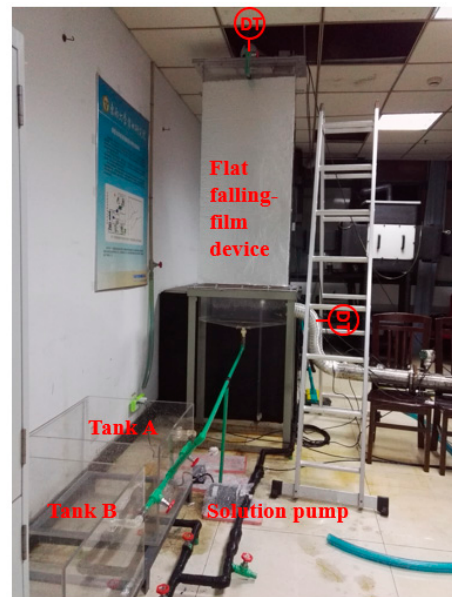


**Figure 3.** A photograph of the flat falling-film experimental device.

**Table 4.** The experimental conditions.

LiCl solution concentration	35%
Solution temperature during dehumidification process	20 °C
Solution temperature during regeneration process	60 °C
Maximum solution flow rate	2 L/min
Maximum air flow rate	129.6 m <sup>3</sup> /h

**Table 5.** The equipment measurement parameters.

Parameter	Equipment	Accuracy	Range
Air flow rate	Gas turbine flowmeter	±1%	12–360 m <sup>3</sup> /h
Solution flow rate	Micro flow turbine sensor Digimesa 939–1525	±2%	0.15–3.74 L/min
Solution temperature	K-type thermocouples	±0.2 °C	−10 to 120 °C
Solution density	Density meter	±0.5 kg/m <sup>3</sup>	1200–400 kg/m <sup>3</sup>

Aerosol refers to a gaseous dispersion system consisting of solid or liquid particles suspended in a gaseous medium. The microparticles contained in the air in this study may include solid particles contained in the treated air or solution microdroplets. According to the definition of an aerosol, it can be judged that the microparticles contained in the treated air are aerosols. In addition, the gas–liquid two-phase flow rate is low in the liquid desiccant air conditioning system, so that the microparticles can settle in the air duct. Studies have shown that particles larger than 10 µm can be rapidly precipitated by their own gravity [30]. Therefore, when considering the problem of indoor air quality, the measurement of microparticles in the air mainly focuses on microparticles with a particle size-range below 10 µm. The TSI DustTrak II 8530 desktop aerosol detector (providing by TSI Corporation in the Shoreview, MN, United States) can measure PM1, PM2.5, PM4, and PM10 in real time. Therefore, to analyze the effect of the heat and mass exchange

between the air and the solution on the contained microparticles, we measure the mass concentration of the microparticles with different particle size ranges in the air at the air inlet and outlet of the device, which is labelled as DT in Figures 1 and 2, using the TSI DustTrak II 8530 desktop aerosol detector. The accuracy of the device is  $0.001 \text{ mg/m}^3$  and the zero drift rate of the device is  $\pm 0.002 \text{ mg/m}^3$ . The mass concentration increment is defined as the  $\Delta C$ , which represents the difference between the mass concentration of particles at the air outlet and that at the air inlet.

### 3. Results and Discussion

#### 3.1. Effect of Air Velocity on Wettability

In this section, the effect of air velocity on the  $WR$  in a parallel flow during the dehumidification and regeneration processes is discussed. The air velocity in the system is mainly below  $1.5 \text{ m/s}$ . The results are shown in Figures 4 and 5. To analyze the reasonable amount of spray, the critical amount of sprays for different air velocities are shown in Table 6. The critical amount of spray is defined as the minimum amount of spray to ensure a full-film flow, as denoted by the dashed lines in Figures 4 and 5.

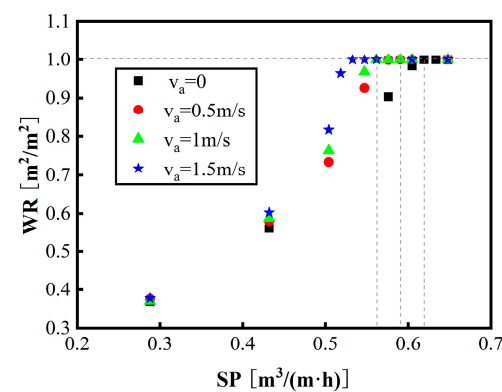


Figure 4. The effect of air velocity on the wetting ratio ( $WR$ ) during dehumidification.

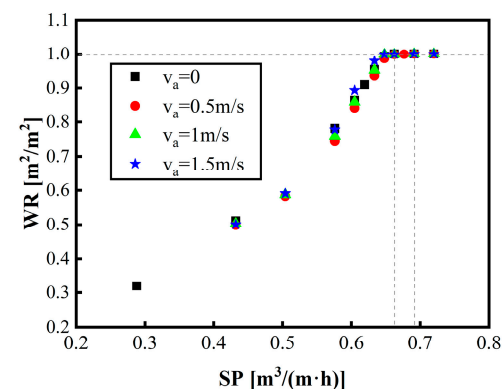


Figure 5. The effect of air velocity on the  $WR$  during regeneration.

Table 6. The critical amount of spray for different air velocities.

Air Velocity (m/s)	Critical Amount of Spray ( $\text{m}^3/(\text{m}\cdot\text{h})$ )	
	Dehumidification	Regeneration
0	0.62	0.66
0.5	0.59	0.69
1	0.59	0.69
1.5	0.56	0.69

For the dehumidification process, Figure 4 shows that before a full-film flow is reached, the  $WR$  increases with increasing air velocity under the same  $SP$ . As seen in Table 6, the larger the air velocity, the smaller the critical spray amount, that is, the better the wettability. This is because the effect of surface tension causes the solution's film to converge toward the center during the flow. When the  $SP$  is small, the effect of surface tension causes the liquid film to form a stream. The shear stress generated by the direction of the air velocity weakens the component of the surface tension that points toward the center, making the liquid film easier to spread. For the regeneration process, Figure 5 shows that before a full-film flow is reached, increasing the air velocity leads to a slight increase in the  $WR$  of the solution under the same  $SP$ . However, the critical amount of spray under a non-air flow is smaller than that where the air velocity is not zero. When the air velocity increases from 0.5 m/s to 1.5 m/s, the critical spray amount remains the same. In general, the air velocity has little effect on the  $WR$  for the regeneration process.

The difference between the dehumidification and regeneration processes is mainly the temperature. The physical properties of the solution (i.e., its density, viscosity, and surface tension) change with its temperature. Surface tension causes the liquid film to converge toward the center, which reduces the wetted area. At the same time, the surface tension also keeps the liquid film stable and not easily broken, which is conducive to the formation of a full-film flow. Viscosity is described as the resistance of the fluid to flow, which prevents the liquid film from converging toward the center during the flow. Therefore, the higher the viscosity, the better the wettability. According to the previous research [24], during dehumidification, surface tension is the major factor that limits wettability. Therefore, the effect of air velocity on the improvement of wettability is apparent. In contrast, during regeneration, viscosity is the major factor that limits wettability. Thus, the air velocity has little effect on the wettability. At the same time, the stability of the liquid film becomes worse when the air velocity is not zero, which will make the critical amount of spray increase.

### 3.2. The Effect of Air Flow Patterns on Wettability

The gas–liquid flow in the flat falling-film liquid desiccant system is mainly divided into parallel flow and counter flow. The simulation results show that the effect of air velocity on the wettability during the dehumidification process for counter flow is the same as that for parallel flow, that is, the greater the air velocity, the better the wettability and the smaller the critical amount of spray. However, the improvement of wettability for counter flow is not as great as that in parallel flow. Figure 6 compares the effect of different flow patterns on the wettability when the flow velocity is 0.5 m/s and 1.5 m/s during the dehumidification process. The dashed lines indicate the critical amount of spray corresponding to the liquid film just reaching a full-film flow, the values of which are given in Table 7.

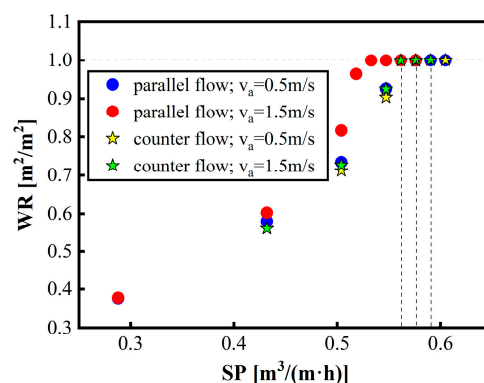


Figure 6. A comparison of the flow patterns at different air velocities under 1 atm.
















**Table 7.** The critical amount of spray for different flow patterns.

Flow Pattern	Air Velocity (m/s)	Critical Amount of Spray ( $\text{m}^3/(\text{m} \cdot \text{h})$ )
Parallel flow	0.5	0.59
Parallel flow	1.5	0.56
Counter flow	0.5	0.59
Counter flow	1.5	0.58

As seen in Figure 6, for dehumidification, when a full-film flow is not reached and the amount of spray is the same, the *WR* increases with increasing air velocity for both flow patterns. However, the wettability of parallel flow (circle point) is markedly improved, whereas the wettability of counter flow (star point) is only slightly improved. Similarly, as seen in Table 7, the critical amount of spray decreases more for the parallel flow when the air velocity increases, whereas the air velocity has little effect on the critical amount of spray for the counter flow. This is because, in the counter flow, a nonzero air velocity hinders the longitudinal spreading of the solution's film and affects its stability. Therefore, the improvement of wettability at high air velocities is much smaller for counter flow than for parallel flow.

The stability of the liquid film at the liquid outlet becomes worse due to the influence of the reverse air velocity, which is evident during the regeneration process. Table 8 compares gas–liquid phase diagrams near a full-film flow during regeneration under a non-air flow, a parallel flow, and a counter flow, where the air velocity is 1.5 m/s. The corresponding *WR* values are shown under each phase diagram. The *WR* that first reaches 1 is marked in red font, the corresponding *SP* of which is the critical amount of spray.

**Table 8.** A diagram of a comparison of the phases of different flow patterns near a full-film flow.

<i>SP</i> ( $\text{m}^3/(\text{m} \cdot \text{h})$ )	0.63	0.66	0.69	0.71	0.72
$v_a = 0$					
<i>WR</i>	0.953	1	1	1	1
Parallel flow $v_a = 1.5 \text{ m/s}$					
<i>WR</i>	0.979	0.999	1	1	1
Counter flow $v_a = 1.5 \text{ m/s}$					
<i>WR</i>	0.936	0.998	0.999	0.999	1

As seen in Table 8, the liquid film immediately reaches a full-film flow with an increasing *SP* in the case where the air velocity is zero. In the case of the parallel flow,

although the decrease in surface tension can improve the wettability during the wetting process ( $SP = 0.63 \text{ (m}^3/(\text{m}\cdot\text{h}))$ ) in Table 6), near full-film flow conditions, the decreased stability will make it difficult to reach a full-film flow, which will increase the critical amount of spray. This situation is even more pronounced in the case of the counter flow. As seen in Table 8, when the liquid phase is close to a full-film flow, the  $WR$  approaches infinitely close to 1 but does not reach a full-film flow as the  $SP$  continues to increase. Therefore, although the air velocity weakens the surface tension to improve the wettability, it also reduces the stability. The adverse effect on stability is especially pronounced at the liquid outlet and air inlet in the case of the counter flow, which increases the critical amount of spray. Furthermore, during the regeneration process, as the air velocity has little effect on the improvement of wettability, the disadvantage of the weakened stability becomes apparent. Therefore, from the viewpoint of wettability, parallel flow is better than counter flow.

### 3.3. Effect of Pressure on Wettability

The research shows that the use of a liquid desiccant in dry compressed air has great energy saving potential, but the current research on solution flow is mainly under atmospheric pressure. The influence of air pressure on the wettability of a solution's flow is still unclear, which brings hidden dangers to the application of compressed air drying using a liquid desiccant. To compare the effect of pressure on wettability more clearly, this section simulates the effect of different pressures on wettability when the liquid film is in a stream-flow state ( $SP = 0.432 \text{ m}^3/\text{m}\cdot\text{h}$ ). The simulation results are shown in Figure 7, which indicate that an increase in pressure has little effect on wettability, even that under different pressures has no effect on the degree of improvement. As for the effect on the critical amount spray, the changes in the  $WR$  with  $SP$  are compared separately under air velocities of 0.5 m/s and 1.5 m/s, and pressures of 1 atm and 8 atm, as shown Figure 8. The corresponding critical spray amounts under different conditions are shown in Table 9.

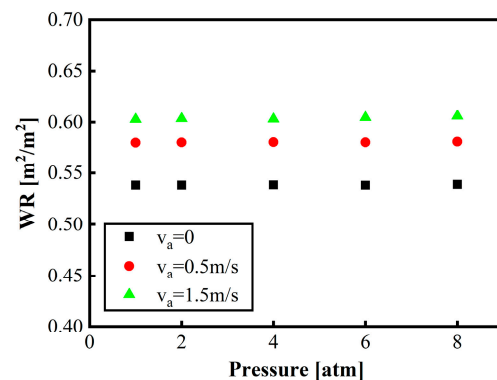


Figure 7. The effect of pressure on wettability under a non-full-film flow.

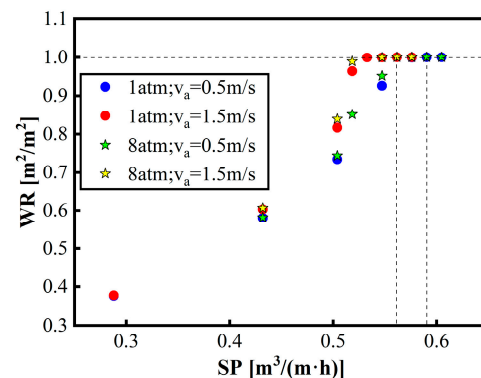


Figure 8. The effect of pressure on the critical amount of spray.

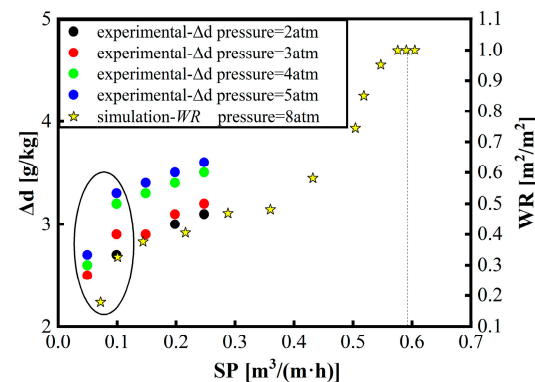


**Table 9.** The critical amount of spray for different air velocities under different pressures.

Pressure (atm)	Air Velocity (m/s)	Critical Amount of Spray ( $\text{m}^3/(\text{m}\cdot\text{h})$ )
1	0.5	0.59
1	1.5	0.56
8	0.5	0.59
8	1.5	0.56

As seen in Figure 8, the wettability under 8 atm is slightly better than that under 1 atm when a full-film flow is not reached. However, the stage where the  $WR$  is close to 1 but does not reach 1 is slightly longer under 8 atm than that under 1 atm; therefore, the critical amount of spray required for the liquid film to reach a full-film flow under 1 atm and 8 atm is the same. Thus, a higher pressure will cause a slight improvement in the wettability before the liquid film reaches a full-film flow, but it has no effect on the critical amount of spray.

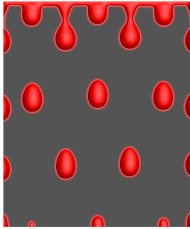
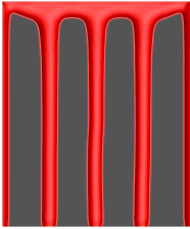
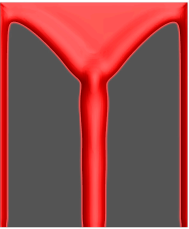
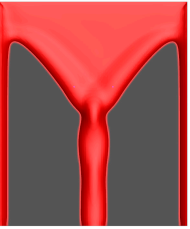
We now compare our simulation results with Yin et al.'s experimental results regarding the effect of the amount of spray on the moisture removal rate during the dehumidification process, as seen in Figure 9 [7,8]. The moisture removal rate is proportional to the mass exchange area. For the flat falling-film liquid desiccant system, the mass exchange area is the area of the solution's film on the surface of the filler. Therefore, the moisture removal rate should be proportional to the  $WR$ . The circle points represent the experimental results of the  $\Delta d$  changing with the  $SP$  under different pressures, and the star points represent the simulation results. As changes in pressure have little effect on wettability, the simulation results of the  $WR$  changing with the  $SP$  under 8 atm are taken as an example for comparative analysis.

**Figure 9.** A comparison between the simulation results and the experimental results of references.

As seen in Figure 9, the  $\Delta d$  increases with the increasing  $SP$  under all pressures. This is because the  $SP$  ranges of the experiment are smaller than the critical amounts of spray. Within the  $SP$  ranges of the experiment, the  $WR$  increases with the increasing  $SP$ , so that the mass exchange area increases. In addition, as indicated by the black circle in Figure 9, when the  $SP$  increases from  $0.05 \text{ m}^3/(\text{m}\cdot\text{h})$  to  $0.1 \text{ m}^3/(\text{m}\cdot\text{h})$ , the growth rate of the  $\Delta d$  is larger, and the  $WR$  also increases significantly. This is because of the changing flow pattern. Table 10 shows the phase diagrams at different  $SP$ s. When the  $SP$  increases from  $0.072 \text{ m}^3/(\text{m}\cdot\text{h})$  to  $0.101 \text{ m}^3/(\text{m}\cdot\text{h})$ , the flow pattern of the liquid film changes from a drop flow to a multiple-streams flow, which results in a stepwise increase in the wettability and the amount of moisture removed. When the  $SP$  increases from  $0.101 \text{ m}^3/(\text{m}\cdot\text{h})$  to  $0.36 \text{ m}^3/(\text{m}\cdot\text{h})$ , the flow state changes from a multiple-streams flow to single-stream flow. Thus, the wettability increases slowly in this range. When the  $SP > 0.36 \text{ m}^3/(\text{m}\cdot\text{h})$ , the flow state is always a single stream until it reaches a full-film flow. When the  $SP$  is within the

experimental range, the simulation results are reasonable for the compressed air drying system using liquid desiccants.

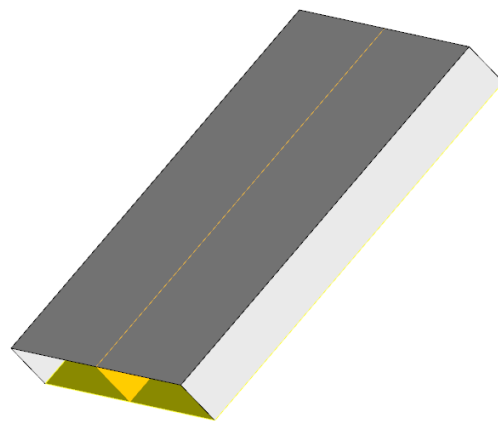
**Table 10.** The phase diagrams of the simulation results at different  $SP$ s.

$SP$ $m^3/(m \cdot h)$	0.072	0.101	0.36	0.59
Phase diagram				

### 3.4. The Effects of Air Parameters on a Solution's Film Stability







We also simulate the solution's falling-film flow process along the flat plate under different air flow parameters. Based on the actual situation in the liquid desiccant air conditioning system, the study mainly simulates the falling-film flow process with an air flow rate of  $<2$  m/s. The solution spray rate is  $0.619 m^3/(m \cdot h)$ , which can form a full-film flow. And the solution condition is the most unfavorable dehumidification condition.

In order to study the solution's film stability, the gas-solution phase diagram on the cross-section of the falling-film plate at the center line in the  $x$  direction was studied. As shown in Figure 10, the yellow surfaces are the falling-film surface and the cross-section taken to research the phase diagram. Table 11 shows the gas-liquid phase diagrams of the falling-film flow process under a counter flow with air flow rates of 1 m/s and 2 m/s, and flow times of 0.1 s, 0.2 s, and 0.3 s. In the phase diagrams of Table 11, red represents the air phase and blue represents the solution phase. The liquid film with an air velocity of 2 m/s at 0.2 s is slightly disturbed at the front end of the liquid film compared to that under an air velocity of 1 m/s due to a significant air flow disturbance. However, due to the flat surface of the liquid film, the high surface tension of the solution, and the low air velocity under the operating conditions, the entire flow process is very stable. When the air flow velocity reaches its maximum (2 m/s), the solution's liquid film will not break due to the shear force of the air flow throughout the entire process. In addition, the simulation results show that the stability of the solution's liquid film is minimally affected under different pressures. The effect of air flow on the stability of the liquid film should be smaller in the counter flow than in the parallel flow. Thus, there will be no liquid film breakage within the given operating range. Therefore, for the flat falling-film flow, the shear force of the airflow is not the main cause of droplet entrainment during the liquid desiccant processes.



**Figure 10.** The cross-section taken to research the phase diagram.

**Table 11.** Phase diagrams of simulation results under different air flow rates.

Time	0.1 s	0.2 s	0.3 s
1 m/s			
			

Considering whether the liquid film will undergo secondary fragmentation due to some accidental droplet impact on the liquid film, the flow evolution of a single droplet's impact on the flowing solution's film was simulated in this study. First, the main factors influencing the flow behavior when droplets hit the flowing solution's film in the operating conditions of the liquid desiccant air conditioning system were analyzed. Table 12 shows the main factors and their value ranges that affect droplet impact behavior. We then simulated each influencing factor separately.

**Table 12.** The main factors influencing droplet impact behavior and their value ranges.

Main Factor	Value Range
Droplet size (mm)	0.4–1.2
Droplet impact velocity (m/s)	0–2
Droplet impact angle	45–90°
Air velocity (m/s)	0–1.5 (Counter flow/Parallel flow)
Solution velocity (m/s)	0–0.6

Figure 11 compares the liquid film morphology at the moment when the liquid film deformation reaches its maximum when droplets of different particle sizes collide with a flowing liquid film. It can be seen that the larger the droplet size, the greater the liquid film's deformation. The liquid film's deformation reaches a maximum when the droplet size is 1.2 mm. At this point, the liquid film is most unstable, but it has not yet broken. The same method is used to study the effects of other factors separately. The results show that when the droplet impact velocity is 2 m/s, the gas–liquid two-phase flow behavior is that of a counter flow, the liquid film impact angle is 45°, the air velocity is 1.5 m/s, and

the solution velocity is 0.6 m/s, in which case the flow pattern of the liquid film is most unstable when droplets collide with it. However, in separate studies of each factor, the liquid film does not break when the impact behavior occurs.

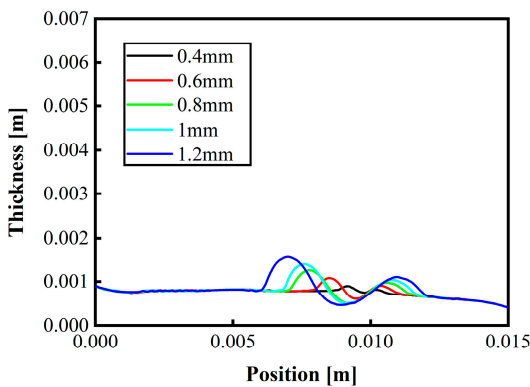
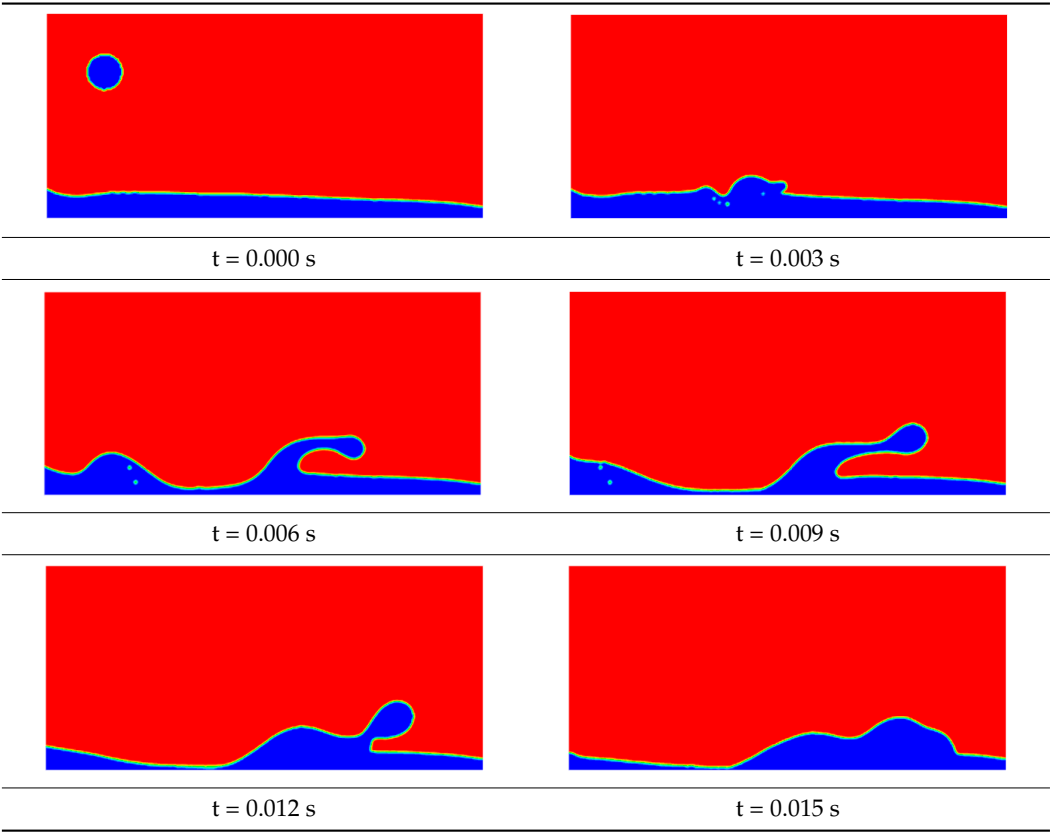


**Figure 11.** Comparison of liquid film morphology when droplets of different sizes collide with a flowing liquid film.

We further simulate the gas–liquid two-phase flow behavior when droplets collide with a flowing liquid film under the most extreme conditions, in which each influencing factor is taken as the value at which the liquid film flow is most unstable when the impact occurs. The simulation results are shown in Table 13. In the phase diagrams of Table 13, red represents the air phase and blue represents the solution phase. It can be seen that during the evolution of a gas–liquid two-phase flow, the difference in neck pressure generated during impact can cause the occurrence of a neck jet. However, due to the high surface tension of LiCl and the low solution flow rate, air flow rate, and droplet impact velocity, no liquid film fragmentation phenomenon occurs.

**Table 13.** The flow evolution of solution droplets impacting a liquid film under extreme conditions.



In addition to this, we also analyze the pressure within the watershed. Figure 12 shows the local phase diagram and pressure distribution when the droplet just hits the liquid film (0.003 s) under extreme conditions. It can be seen that due to the small impact velocity, the pressure difference generated is approximately 3000 Pa, which is much smaller than the 70,000 Pa found in the literature (the impact velocity in the literature is 10 m/s). In addition, the surface tension of the solution is higher than that of water; thus, there are no microdroplets generated due to the secondary fragmentation of the droplets.

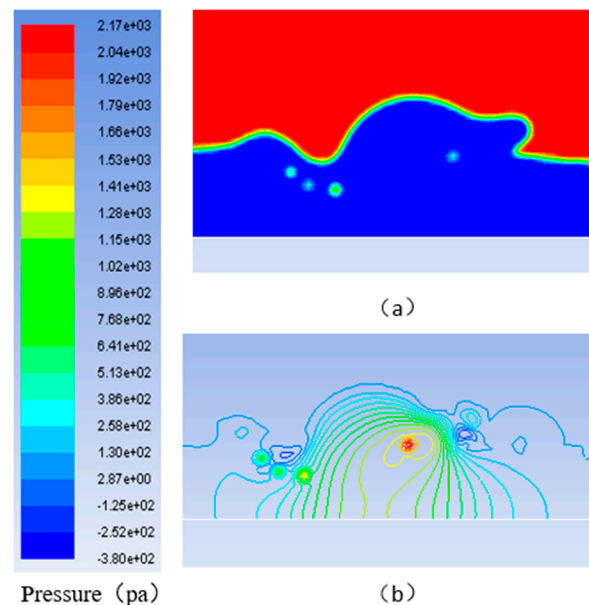


**Figure 12.** (a) A local phase diagram. (b) The local pressure distribution when a droplet hits the liquid film under extreme conditions.

To further validate the simulation results, we experimentally measured the mass concentration increment of the microparticles in the air before and after the dehumidification and regeneration processes at air volumes of 32.4 m<sup>3</sup>/h, 64.8 m<sup>3</sup>/h, 97.2 m<sup>3</sup>/h, and 129.6 m<sup>3</sup>/h. According to the previous research, the solution mainly absorbs particles with a diameter of 0–2.5 µm and releases particles with diameters of 2.5–10 µm [31]. Therefore, the size range of the microparticles analyzed in this part of the study is reduced to 2.5–10 µm. Define  $\Delta C_{2.5-10\mu\text{m}}$  to represent the  $\Delta C$  of the microparticles with a diameter of 2.5–10 µm. If the shear force of the air flow produces droplet entrainment, the  $\Delta C_{2.5-10\mu\text{m}}$  will increase with the increasing air flow rate. Figure 13 compares the  $\Delta C_{2.5-10\mu\text{m}}$  in the air at different air flow rates after the dehumidification and regeneration processes.

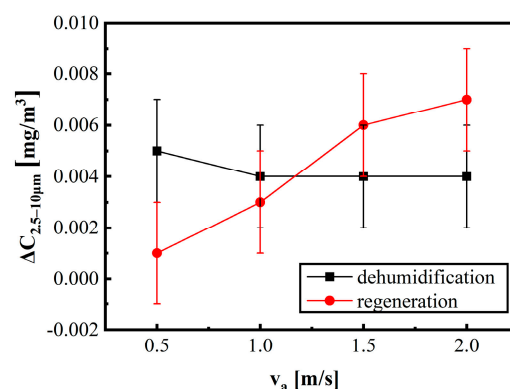


**Figure 13.** The effect of the airflow rate on the  $\Delta C_{2.5-10\mu\text{m}}$  of microparticles.

As can be seen from Figure 13, for the dehumidification process, the  $\Delta C_{2.5-10\mu m}$  is  $0.005 \text{ mg/m}^3$  when the air flow rate is  $0.5 \text{ m/s}$ . When the air flow rate increases to  $1 \text{ m/s}$ , the  $\Delta C_{2.5-10\mu m}$  decreases to  $0.004 \text{ mg/m}^3$ . When the air flow rate continues to increase, the  $\Delta C_{2.5-10\mu m}$  does not change. Considering that the measuring instrument also exists at  $\pm 0.002 \text{ mg/m}^3$  of zero drift, the dehumidification process has little effect on the microparticles. For the regeneration process, the  $\Delta C_{2.5-10\mu m}$  increases with the increase in the air flow rate. Therefore, the experimental results indicated that the increase in microparticles is not directly related to changes in the air flow rate, but rather to the air treatment process. The higher the airflow rate, the greater the shear force of the airflow. This indicates that the shear force of the air flow is not the main reason for the release of microdroplets in the liquid desiccant of flat falling-film solutions, which is consistent with the simulation results.

#### 4. Conclusions

To control droplet entrainment while improving the efficiency of the liquid desiccant air conditioning systems, this work mainly discusses the effects of air velocity, the air flow pattern, and pressure on the wettability and stability characteristics of the system during dehumidification and regeneration using  $\text{LiCl-H}_2\text{O}$ . The major conclusions of this work are as follows:

1. In terms of the film wettability, the main reason that the air velocity affects the wettability is that the shear stress generated by the direction of the air velocity disperses the direction of the surface tension and weakens its effect on the liquid film distribution. During dehumidification, the surface tension is the main factor that makes the wettability worse. Thus, the effect of air velocity on the improvement of wettability during dehumidification is apparent: the higher the air velocity, the better the wettability and the smaller the critical amount of spray. During regeneration, because the viscosity is the main factor that makes the wettability worse, the air velocity has little effect on the wettability. The gas-phase flow blocks the longitudinal spreading of the liquid film and destroys the stability of the liquid film in the counter flow. The adverse effect on stability is especially pronounced at the liquid outlet and the air inlet, which increases the critical amount of spray in the counter flow pattern. Therefore, from the viewpoint of wettability, parallel flow is better than counter flow. The pressure distribution is similar under different operating pressures when the flow is stable, and the differential pressures under different operating pressures are also very similar. Therefore, changing the pressure leads to a weak improvement in wettability but has no effect on the critical amount of spray. By comparing the simulation data under  $8 \text{ atm}$  with the experimental data from Yin et al. [7,8], it is found that the sudden increase in the amount of moisture removal when the  $SP$  changes from  $0.05 \text{ m}^3/(\text{m}\cdot\text{h})$  to  $0.1 \text{ m}^3/(\text{m}\cdot\text{h})$  in the experiment is caused by the change in the liquid film flow state.

2. In terms of the film stability, the simulation results show that the front end of the liquid film will be slightly disturbed by the shear force of the air flow during the falling-film process. In addition, the disturbance of the counter flow is greater than that of the parallel flow. However, due to the stable shape of the flat falling film, the larger surface tension of a salt solution and the smaller air flow rate, the shear force of the air will not break the liquid film. The experimental results also show that increasing the air flow rate during dehumidification does not increase the  $\Delta C_{2.5-10\mu m}$ . Therefore, for a flat falling-film flow, the shear force of the air flow is not the main cause of droplet entrainment during the dehumidification and regeneration processes. In addition, when a droplet collides with a flowing liquid film under the most extreme conditions, due to the high surface tension of  $\text{LiCl}$  and the low solution flow rate, air flow rate, and droplet impact velocity, the difference in neck pressure generated by the impact is far from the threshold for causing the solution's film to break. Thus, no liquid film secondary fragmentation phenomenon occurs during the liquid desiccant processes.



**Author Contributions:** Conceptualization, Y.L. and Y.Y.; data curation, Y.L.; investigation, Y.L.; resources, Y.L. and J.W.; software, Y.L.; validation, Y.L.; writing—original draft, Y.L.; writing—review and editing, Y.L. and J.W. All authors have read and agreed to the published version of the manuscript.

**Funding:** This research was funded by the Gansu Province Youth Science and Technology Fund Program, grant number 22JR5RA371.

**Data Availability Statement:** The data presented in this study are available on request from the corresponding author.

**Conflicts of Interest:** The authors declare no conflicts of interest.

## Nomenclature

$A_b$ —the area of the mainly plate, [m<sup>2</sup>]  
 $A_w$ —the projection area of liquid film on the board, [m<sup>2</sup>]  
 $\Delta d$ —the difference of the air moisture content between the inlet and outlet, [g/kg]  
 $F$ —the force, [N]  
 $Q$ —volumetric flow rate of liquid, [m<sup>3</sup>/s]  
 $SP$ —the amount of spray, which is the volumetric flow rate per unit length per unit time, [m<sup>3</sup>/(m·h)]  
 $v$ —the velocity, [m/s]  
 $W$ —the inlet width, [m]  
 $WR$ —the wetting ratio, [m<sup>2</sup>/m<sup>2</sup>]  
 $\Delta C$ —The mass concentration increment, [mg/m<sup>3</sup>]  
 Greek symbol  
 $\alpha$ —the volume fraction, [–]  
 $\kappa$ —the curvature, [m<sup>−1</sup>]  
 $\mu$ —viscosity, [Pa·s]  
 $\rho$ —density, [kg/m<sup>3</sup>]  
 $\sigma$ —surface tension, [mN/m]  
 Subscripts  
 $a$ —air  
 $s$ —solution  
 $vol$ —volume

## References

1. Bazdar, E.; Sameti, M.; Nasiri, F.; Haghighat, F. Compressed air energy storage in integrated energy systems: A review. *Renew. Sustain. Energy Rev.* **2022**, *167*, 112701. [\[CrossRef\]](#)
2. Nehler, T. Linking energy efficiency measures in industrial compressed air systems with non-energy benefits—A review. *Renew. Sustain. Energy Rev.* **2018**, *89*, 72–87. [\[CrossRef\]](#)
3. Sureshkannan, V.; Vijayan, S.; Lenin, V.R. Design and performance analysis of compressed air adsorption dryer with heatless regeneration mode. *Heat Mass Transf.* **2022**, *58*, 631–641. [\[CrossRef\]](#)
4. Su, W.; Lu, Z.F.; She, X.H.; Zhou, J.M.; Wang, F.; Sun, B.; Zhang, X.S. Liquid desiccant regeneration for advanced air conditioning: A comprehensive review on desiccant materials, regenerators, systems and improvement technologies. *Appl. Energy* **2022**, *308*, 118394. [\[CrossRef\]](#)
5. Luo, J.L.; Yang, H.X. A state-of-the-art review on the liquid properties regarding energy and environmental performance in liquid desiccant air-conditioning systems. *Appl. Energy* **2022**, *325*, 119853. [\[CrossRef\]](#)
6. Oladosu, T.L.; Baheta, A.T.; Oumer, A.N. Desiccant solutions, membrane technologies, and regeneration techniques in liquid desiccant air conditioning system. *Int. J. Energy Res.* **2021**, *45*, 8420–8447. [\[CrossRef\]](#)
7. Yin, Y.G.; Zheng, B.J.; Yang, C.; Zhang, X.S. A proposed compressed air drying method using pressurized liquid desiccant and experimental verification. *Appl. Energy* **2015**, *141*, 80–89. [\[CrossRef\]](#)
8. Yin, Y.; Shao, B.; Zhang, X.S. Experimental investigation on compressed air drying performance using pressurized liquid desiccant. *Dry. Technol.* **2016**, *34*, 372–382. [\[CrossRef\]](#)
9. Peng, D.G.; Xu, S.H.; Yang, H.X. Heat and Mass Transfer Characteristics and Dehumidification Performance Improvement of an Evaporatively-Cooled Liquid Dehumidifier. *Appl. Therm. Eng.* **2020**, *178*, 115579. [\[CrossRef\]](#)
10. Liu, X.L.; Qu, M.; Liu, X.B.; Wang, L.S. Membrane-based liquid desiccant air dehumidification: A comprehensive review on materials, components, systems and performances. *Renew. Sustain. Energy Rev.* **2019**, *110*, 444–466. [\[CrossRef\]](#)
11. Mandow, W.; Micus, F.; Völker, L.; Fleig, D.; Jordan, U. Solar driven liquid desiccant dehumidification system: Measurements and annual system simulations. *Appl. Therm. Eng.* **2024**, *242*, 122485. [\[CrossRef\]](#)

12. Lee, J.H.; Cheon, S.Y.; Lee, S.J.; Cho, H.J.; Jeong, J.W. Applicability of a liquid-desiccant air-conditioning system in energy-efficient buildings with high latent load. *J. Build. Eng.* **2023**, *78*, 107608. [\[CrossRef\]](#)
13. Mortazavi, M.; Isfahani, R.N.; Bigham, S.; Moghaddam, S. Absorption characteristics of falling film LiBr (lithium bromide) solution over a finned structure. *Energy* **2015**, *87*, 270–278. [\[CrossRef\]](#)
14. Zhao, C.Y.; Zhang, P.; Guan, Q.; Qi, D.; Zhang, Y.; Jiang, J.M. Numerical study of falling film dehumidification performance on corrugated plates. *Int. J. Heat Mass Transf.* **2024**, *219*, 124843. [\[CrossRef\]](#)
15. Lu, X.B.; Liu, J.P.; Xu, X.W.; Chen, J.X. Change in wetting characteristic of heated refrigerant in falling film evaporation. *Int. J. Refrig.* **2020**, *117*, 198–208. [\[CrossRef\]](#)
16. Sakhnov, A.Y.; Volodin, O.A.; Pecherkin, N.I.; Pavlenko, A.N. Effect of contact angle on spreading of refrigerant mixture over the vertical cylinder. *Int. J. Heat Mass Transf.* **2023**, *215*, 124484. [\[CrossRef\]](#)
17. Kuznetsov, D.V.; Pavlenko, A.N.; Volodin, O.A. Effect of structuring by deformational cutting on heat transfer and dynamics of transient cooling processes with liquid film flowing onto a copper plate. *J. Eng. Thermophys.* **2020**, *29*, 531–541. [\[CrossRef\]](#)
18. Tan, L.Y.; Yuan, X.G.; Kalbassi, M.A. Computational fluid dynamics study of liquid distribution on structured packing surface. *Chem. Ind. Eng. Prog.* **2015**, *34*, 3221–3237.
19. Wen, T.; Luo, Y.M.; He, W.F.; Gang, W.J.; Sheng, L.Y. Development of a novel quasi-3D model to investigate the performance of a falling film dehumidifier with CFD technology. *Int. J. Heat Mass Transf.* **2019**, *132*, 431–442. [\[CrossRef\]](#)
20. Zhang, L.; Hihara, E.; Matsuoka, F.; Dang, C. Experimental analysis of mass transfer in adiabatic structured packing dehumidifier/regenerator with liquid desiccant. *Int. J. Heat Mass Transf.* **2010**, *53*, 2856–2863. [\[CrossRef\]](#)
21. Yu, D.; Cao, D.P.; Li, Z.Z.; Li, Q.S. Experimental and CFD studies on the effects of surface texture on liquid thickness, wetted area and mass transfer in wave-like structured packings. *Chem. Eng. Res. Des.* **2018**, *129*, 170–181. [\[CrossRef\]](#)
22. Wang, B.; Ke, B.Z.; Chen, B.W.; Li, R.; Tian, R. Study on the size of secondary droplets generated owing to rupture of liquid film on corrugated plate wall. *Int. J. Heat Mass Transf.* **2020**, *147*, 118904. [\[CrossRef\]](#)
23. Dai, J.F.; Fan, X.P.; Meng, B.; Liu, J.F. A coupled level-set and volume-of-fluid simulation for splashing of single droplet impact on an inclined liquid film. *Acta Phys. Sin.* **2015**, *64*, 094704.
24. LYu, Y.; Yin, Y.G.; Zhang, X.S.; Jin, X. Investigation of falling-film plate wettability characteristics under dehumidification and regeneration conditions using LiCl-H<sub>2</sub>O. *Int. J. Refrig.* **2018**, *94*, 118–126. [\[CrossRef\]](#)
25. Van der Graaf, S.; Nisisako, T.; Schroën, C.G.P.H.; van der Sman, R.G.M.; Boom, R.M. Lattice Boltzmann simulations of droplet formation in a T-shaped microchannel. *Langmuir* **2006**, *22*, 4144–4152. [\[CrossRef\]](#)
26. Pozrikidis, C. Interfacial dynamics for Stokes flow. *J. Comput. Phys.* **2001**, *169*, 250–301. [\[CrossRef\]](#)
27. Taha, T.; Cui, Z.F. CFD modelling of slug flow in vertical tubes. *Chem. Eng. Sci.* **2006**, *61*, 676–687. [\[CrossRef\]](#)
28. Taha, T.; Cui, Z.F. CFD modelling of slug flow inside square capillaries. *Chem. Eng. Sci.* **2006**, *61*, 665–675. [\[CrossRef\]](#)
29. Brackbill, J.U.; Kothe, D.B.; Zemach, C. A continuum method for modeling surface tension. *J. Comput. Phys.* **1992**, *100*, 335–354. [\[CrossRef\]](#)
30. Huang, S.; Xu, J.; Liang, C.; Zhang, X. Size distribution measurement of packed tower drift based on hydrophobic materials. *Appl. Therm. Eng.* **2016**, *99*, 873–879. [\[CrossRef\]](#)
31. LYu, Y.; Yin, Y.G.; Zhao, X.W.; Zhang, C.B. Effects of liquid-desiccant air conditioning processes on the presence of inhalable particles in the air. *Build. Environ.* **2021**, *194*, 107662.

**Disclaimer/Publisher’s Note:** The statements, opinions and data contained in all publications are solely those of the individual author(s) and contributor(s) and not of MDPI and/or the editor(s). MDPI and/or the editor(s) disclaim responsibility for any injury to people or property resulting from any ideas, methods, instructions or products referred to in the content.